Experimental Characterization of Bosonic Creation and Annihilation Operators

R. Kumar, E. Barrios, and C. Kupchak
Institute for Quantum Information Science, University of Calgary, Calgary, Canada T2N 1N4

A. I. Lvovsky*
Institute for Quantum Information Science, University of Calgary, Calgary, Canada T2N 1N4 and Russian Quantum Center, 100 Novaya Street, Skolkovo, Moscow 143025, Russia
(Received 3 November 2012; published 25 March 2013)

The photon creation and annihilation operators are cornerstones of the quantum description of the electromagnetic field. They signify the isomorphism of the optical Hilbert space to that of the harmonic oscillator and the bosonic nature of photons. We perform complete experimental characterization (quantum process tomography) of these operators. By measuring their effect on coherent states by means of homodyne tomography, we obtain their process tensor in the Fock basis, which explicitly shows the "raising" and "lowering" properties of these operators with respect to photon number states. This is the first experimental demonstration of complete tomography of nondeterministic quantum processes.

DOI: 10.1103/PhysRevLett.110.130403 PACS numbers: 03.65.Wj, 03.65.Ta, 42.50.Xa

Introduction.—Quantum operators of annihilation $\hat{a}$ and creation $\hat{a}^\dagger$ of bosonic particles act on states with a definite number m of identical particles, resulting in that number being incremented or decremented, respectively:

$$\hat{a}^\dagger|m\rangle = \sqrt{m+1}|m+1\rangle, \qquad \hat{a}|m\rangle = \sqrt{m}|m-1\rangle. \quad (1)$$

First proposed by Dirac in 1927 [1], these operators play a major role in many fields of physics and chemistry: quantum mechanics, quantum optics, quantum chemistry, quantum field theory, and condensed matter physics. Specializing to optics, they are instrumental in the quantum description of light, giving rise to many fundamental phenomena such as spontaneous emission, Lamb shift, Casimir force, and lasing. Equally important is practical implementation of photon creation and annihilation, which provides a necessary component of a universal toolbox for manufacturing arbitrary quantum states of light, required for quantum information processing and quantum communications [2,3].

Implementation of $\hat{a}$ and $\hat{a}^\dagger$ is, however, challenging. This is because these operators do not preserve the trace of a state's density matrix, which means they cannot occur in the framework of deterministic Hamiltonian evolution of a physical system. Therefore, bosonic creation and annihilation can be realized in the laboratory only in an approximate, nondeterministic fashion. That is, the action of the operators occurs with probability less than one, but is heralded by a classical event.

One possible realization of photon annihilation in optics employs a low reflectivity beam splitter, through which the target state $|\psi\rangle$ is transmitted [Fig. 1(a)]. Detection of a single photon in the reflection channel indicates that this photon has been removed from state $|\psi\rangle$. In this case, the state emerging in the transmission channel of the beam splitter is approximated by $\hat{a}|\psi\rangle$.

Photon creation can be achieved using low-amplitude spontaneous parametric down-conversion (SPDC) in a nonlinear optical crystal. The target state enters the signal SPDC mode from the back of the crystal [Fig. 1(b)]. When SPDC occurs, operators $\hat{a}^\dagger$ act simultaneously on both the signal and the idler modes. If this event is heralded by the photon detector in the idler channel, the target state becomes $\hat{a}^\dagger|\psi\rangle$ [4].

The first successful realization of the optical photon creation operator in this manner in 2004 [5] gave rise to a new class of states known as photon added state. In 2006, Ourjoumtsev and colleagues applied the photon annihilation operation to the squeezed states generating optical superpositions called cat states [6]. Neergaard-Nielsen *et al.* generalized this approach in 2010 to generating arbitrary continuous-variable qubits [7]. In 2007, Parigi *et al.* verified noncommutativity of $\hat{a}$ and $\hat{a}^\dagger$ in application to the thermal state [8]. The photon annihilation operator has been used for continuous-variable entanglement distillation in 2010 by Takahashi and co-workers [9]. Experimental recording of photon creation and annihilation events in the time domain has been reported by Gleyzes *et al.* [10].

The present work offers an experimental study of $\hat{a}$ and $\hat{a}^\dagger$ as quantum "black boxes," or quantum processes. By

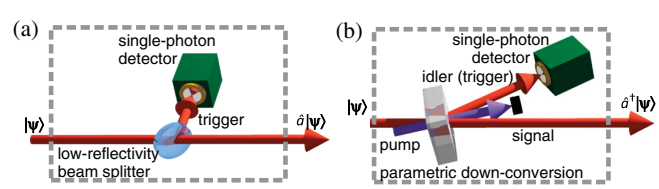

FIG. 1 (color online). Experimental setups for photon annihilation (a) and creation (b). The processes are heralded by "clicks" in single-photon detectors.

probing them with coherent optical states (weak laser pulses) of different amplitudes and subjecting the output electromagnetic field to optical homodyne tomography [11,12], we determine how these black boxes would affect any arbitrary state of light within a practically relevant subspace of the optical Hilbert space. As a result, we explicitly observe their action on the photon number states to be in accordance with Eq. (1).

Coherent-state quantum-process tomography.—Our method of characterizing quantum processes relies on the optical equivalence theorem. According to that theorem, the density operator $\hat{\rho}$ of an arbitrary state can be written as a linear combination of coherent-state density operators,

$$\hat{\rho} = \int P_{\hat{\rho}}(\alpha)|\alpha\rangle\langle\alpha| d^2\alpha, \tag{2}$$

where $P_{\hat{\rho}}(\alpha)$ is the Glauber-Sudarshan P function of state $\hat{\rho}$. Further, since every quantum process $\mathcal{E}$ (in this case, photon creation and annihilation) is a linear map with respect to density matrices, we can write the process output as

$$\mathcal{E}(\hat{\rho}) = \int P_{\hat{\rho}}\mathcal{E}(|\alpha\rangle\langle\alpha|) d^2\alpha. \tag{3}$$

If we know $\mathcal{E}(|\alpha\rangle\langle\alpha|)$ for every coherent state $|\alpha\rangle$, we can determine the process output $\mathcal{E}(\hat{\rho})$ for any state $\hat{\rho}$.

This is of benefit because optical states used in quantum information processing (for example, number states or their superpositions) are highly nonclassical and cannot be generated easily. In contrast, coherent states are directly obtained from lasers. Our method permits us, by probing the black box with regular laser pulses, to learn its effect on any other state of light, however complicated it may be. Previously, this approach, referred to as coherent-state quantum process tomography (csQPT) [13–15], has been applied to the processes of attenuation, phase shift [13], and quantum optical memory [16]. A closely related method has been used for the quantum characterization of optical detectors [17–20].

The result of csQPT—the data about the process—can be compactly written in the form of a *process tensor.* This is a rank-4 tensor $\mathcal{E}_{jk}^{mn}$ such that, for any process input $\hat{\rho}$, the density operator of the process output in the photon number basis is given by $[\mathcal{E}(\hat{\rho})]_{jk} = \sum_{m,n}\mathcal{E}_{jk}^{mn}\hat{\rho}_{mn}$. The process tensor is calculated according to

$$\mathcal{E}_{jk}^{mn} = \int P_{mn}(\alpha)\langle j|\mathcal{E}(|\alpha\rangle\langle\alpha|)|k\rangle d^2\alpha, \tag{4}$$

where $P_{mn}(\alpha)$ is the P function of operator $|m\rangle\langle n|$. Computation of the process tensor is complicated by the highly singular nature of this function; Refs [13–15,21] elaborate different ways of resolving this complication. Another practical issue is associated with the infinite dimension of the optical Hilbert space. In csQPT experiments, the process tensor is evaluated for a subspace $\mathcal{H}(n_{\max})$ spanned by number states up to a certain cutoff value, $n_{\max}$. The choice of $n_{\max}$ is determined by the maximum amplitude $\alpha_{\max}$ of the set of coherent probe states used in the experiment, as well as the reconstruction method used. In our work, $n_{\max} = 7$.

Experiment.—The primary light source is a mode-locked Ti:sapphire laser (Coherent Mira 900), which emits transform-limited pulses at ~790 nm with a repetition rate of 76 MHz and a pulse width of ~1.6 ps. Heralding photons are registered by PerkinElmer SPCM-AQR-14-FC single-photon detectors. The field quadratures of the output states are measured by means of high-bandwidth balanced homodyne detectors [12,22,23]. Both the probe field and the local oscillator field for homodyne detection are obtained from the master laser. The amplitude of the probe field is controlled by a set of half-wave plates, polarizers and attenuators.

In order to obtain SPDC, required for the photon creation, the light from the master laser is frequency doubled in a single pass through a 17-mm long lithium triborate crystal, yielding a typical ~80 mW average second-harmonic power after spatial filtering. This field is focused, with a waist of 100 μm, into a 2-mm long periodically poled potassium-titanyl phosphate crystal phase matched for type II SPDC. The signal and idler modes are spatially and spectrally degenerate but are of orthogonal polarization [24,25].

State transformation.—We acquire a set of field quadrature data for the outputs of both processes for a set of probe coherent states with amplitudes ranging from 0 to about 1 [4]. For the photon annihilation process, the output states are almost identical to the input states, as they only undergo slight attenuation in the beam splitter [Fig. 1(a)]. This is to be expected, because coherent states are eigenstates of $\hat{a}$. Photon creation, on the other hand, significantly changes the character of the input state, producing highly nonclassical single-photon added coherent states, studied in detail theoretically by Agarwal and Tara [26], experimentally by Zavatta and co-workers [5,8].

The processes we study are nondeterministic, and their probability of occurrence depends on the input state. Accounting for this dependence is crucial for the correct reconstruction. In csQPT, this is done by renormalizing the process output for the probe states so that $\mathrm{Tr}[\mathcal{E}(|\alpha\rangle\langle\alpha|)]$ in Eqs. (3) and (4) is proportional to the probability of the heralding event [14]. To illustrate the significance of this step, it is instructive to apply Eq. (3) to the photon annihilation operator, such that $\mathcal{E}(|\alpha\rangle\langle\alpha|) = |\alpha|^2|\alpha\rangle\langle\alpha|$. If the coefficient $|\alpha|^2$, responsible for the nondeterministic nature of $\hat{a}$, is neglected, we would obtain the identity process. Hence, remarkably, the "lowering" feature of $\hat{a}$ arises in csQPT due to the variation of the event probability as a function of the probe amplitude, rather than transformation of the probe state itself.

The information on the heralding event probability is obtained by keeping track of the photon count rates for various input states. Theoretically, we expect these rates to behave as

$$\begin{aligned} \mathrm{pr}_{\hat{a}}(\alpha) &\propto \langle\alpha|\hat{a}^\dagger\hat{a}|\alpha\rangle = \alpha^2; \\ \mathrm{pr}_{\hat{a}^\dagger}(\alpha) &\propto \langle\alpha|\hat{a}\hat{a}^\dagger|\alpha\rangle = 1 + \alpha^2. \end{aligned} \tag{5}$$

The experimentally observed dependencies are consistent with these expectations as displayed in Fig. 2.

We use an iterative algorithm, elaborated theoretically in Ref. [15], to reconstruct the process tensors directly from the acquired field quadrature data. The algorithm makes use of the Jamiolkowski isomorphism between quantum processes applied to Hilbert space $\mathcal{H}$ and positive semidefinite operators over the Hilbert space $\mathcal{H} \otimes \mathcal{H}$ [27]. In this way, the task of process reconstruction is reduced to the known problem of state reconstruction [12,28–30]. This scheme guarantees that the resulting process is physically consistent, i.e., completely positive. Furthermore, it permits us to incorporate correction for experimental imperfections into the reconstruction procedure, as we discuss next.

Accounting for experimental imperfections.—Under such imperfections we understand known factors that distort the measurement of the process output. For the annihilation operator $\hat{a}$, these factors are the linear losses, nonunitary quantum efficiency, and the electronic noise of the homodyne detector [31]. All these effects can be quantified and their cumulative contribution can be modeled by an attenuator with transmission $T_1 = 0.75$ placed after a black box containing an ideal photon annihilation operator [Fig. 3(a)]. This attenuator is accounted for in maximum-likelihood homodyne reconstruction by modifying the measurement operator associated with detecting field quadrature values [11,15,28].

For the photon creation, one must additionally account for the mode mismatch between the probe field and the signal mode of parametric down-conversion, which is determined by the mode of the pump and the optics in the idler channel [32]. This mismatch is modeled by a Mach-Zehnder interferometer with beam splitting ratio T_2 and an ideal photon creation operator placed into one of its arms [Fig. 3(b), top]. To determine T_2, we observe that, when the input $|\alpha_{\mathrm{in}}\rangle$ is in the vacuum state, the output is expected to be a statistical mixture of the single-photon and vacuum states, with the single-photon fraction equal to T_1T_2. The output observed experimentally in this case is indeed, to a high degree of precision, described by such a mixture [24,33], with the single-photon fraction equal to 0.59. Knowing that $T_1 = 0.75$, we conclude that $T_2 = 0.59/0.75 = 0.79$. With this model, if the coherent state entering the interferometer is $|\alpha_{\mathrm{in}}\rangle$, the state entering the black box is $|\alpha\rangle = |\sqrt{T_2}\alpha_{\mathrm{in}}\rangle$. The latter is the amplitude that we refer to in Fig. 2(b) and use in all calculations associated with evaluating the process tensor of the photon creation operator.

This model is corroborated by the photon statistics observed in Fig. 2(b). The least-squares fit to the experimental data yields $\mathrm{pr}_{\hat{a}^\dagger}(\alpha) \propto 1 + 0.98\alpha^2$, which is close to the theoretically expected $\mathrm{pr}_{\hat{a}^\dagger}(\alpha) \propto 1 + \alpha^2$.

It is convenient to reformulate the Mach-Zehnder interferometer model in terms of the equivalent scheme shown in the bottom panel of Fig. 3(b). The output of the black box undergoes a linear loss channel with transmissivity T_1T_2 followed by phase-space displacement by $\Delta X = \sqrt{2T_1}(1 - T_2)\alpha_{\mathrm{in}}$. Therefore, prior to launching the iterative algorithm with correction for a linear loss, we apply inverse displacement to the measured quadrature data. Namely, we subtract $\Delta X \cos\theta$ from each experimentally measured sample of quadrature observable $\hat{X}_\theta = \hat{X}\cos\theta + \hat{P}\sin\theta$, where θ is the local oscillator phase.

Process reconstruction.—In order to apply the Jamiolkowski isomorphism to the reconstruction of nondeterministic processes, we introduce an additional, fictitious state $|\varnothing\rangle$ into the Hilbert space. The process can then be treated as deterministic: events in which no "click"

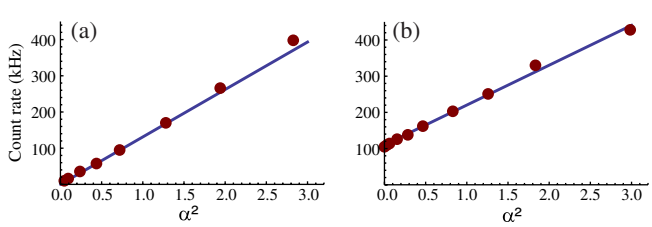

FIG. 2 (color online). Event count rate for the photon annihilation (a) and creation (b) operators as a function of the input coherent state amplitudes in the modes to which these operators are applied. The solid lines show the expected theoretical dependencies (5), with the vertical scale fit to the data.

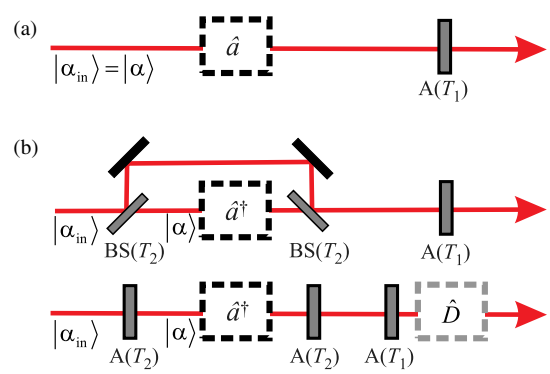

FIG. 3 (color online). Model of experimental imperfections for the photon annihilation (a) and creation (b) setups. The top and bottom schemes in (b) are equivalent to each other. Notation: BS, beam splitter; A, attenuator; the quantities in parentheses denote the transmission of the corresponding optical element. $\hat{D}$ denotes the operator of phase-space displacement by $\Delta X = \sqrt{2T_1}(1 - T_2)\alpha_{\mathrm{in}}$. The amplitude of the input coherent probe state is α_{in} while α is the effective amplitude of the coherent state in the mode acted upon by the operators.

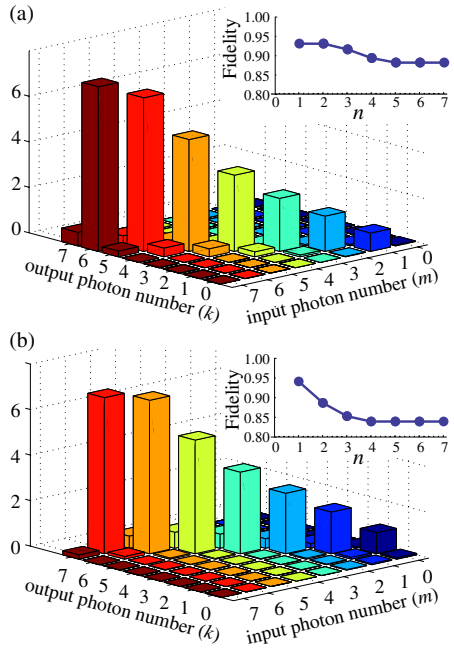

FIG. 4 (color online). The "diagonal" values of the process tensor ε_{kk}^{mm} of the photon annihilation (a) and creation (b) reconstructed from the experimental data, with correction for experimental imperfections. Each color corresponds to the photon number distribution in the output state for the Fock state $|m\rangle$ at the input. Insets: Worst-case fidelities of the reconstructed processes acting within subspaces $\mathcal{H}'_{\hat{a},\hat{a}^\dagger}(n)$ of the optical Hilbert space spanned by number states $|1\rangle, \ldots, |n\rangle$ and $|0\rangle, \ldots, |n-1\rangle$, for $\hat{a}$ and $\hat{a}^\dagger$, respectively.

occurred are interpreted as events in which the process has generated state $|\varnothing\rangle$ in the output [14,27].

The reconstruction algorithm converges after about 2000 iterations. The diagonal elements $\mathcal{E}_{kk}^{mm}$ of the obtained process tensors are shown in Fig. 4. These elements permit straightforward interpretation: they give the probability that the output of the quantum black box contains k photons when the m-photon state is present at the input. According to Eq. (1), we expect $(\mathcal{E}_{\hat{a}})_{kk}^{mm} = m\delta_{k,m-1}$ and $(\mathcal{E}_{\hat{a}^\dagger})_{kk}^{mm} = (m+1)\delta_{k,m+1}$. The experimental result is consistent with this expectation and explicitly features the "raising" and "lowering" properties of $\hat{a}^\dagger$ and $\hat{a}$. For input state $|m\rangle$, the output state is similar to $|m+1\rangle$ for operator $\hat{a}^\dagger$ and $|m-1\rangle$ for operator $\hat{a}$. The height of the bars in the plots increases linearly with m, which is associated with the squared factors $\sqrt{m+1}$ and $\sqrt{m}$ in the right-hand sides of Eq. (1).

The consistency of the estimated process tensors with those theoretically expected can be quantified using the fidelity benchmark. We estimate the worst-case fidelity between normalized states $\hat{a}|\psi\rangle$, $\hat{a}^\dagger|\psi\rangle$ and the respective outputs $\mathcal{E}_{\hat{a},\hat{a}^\dagger}(|\psi\rangle\langle\psi|)$ of the reconstructed processes. The processes are applied to pure states within subspaces $\mathcal{H}'_{\hat{a},\hat{a}^\dagger}(n)$ of the optical Hilbert space spanned by number states $|1\rangle, \ldots, |n\rangle$ and $|0\rangle, \ldots, |n-1\rangle$, respectively, with n ranging between 1 and $n_{\max}$. For each n, we employ the genetic algorithm to identify the input state producing the lowest fidelity in $\mathcal{H}'_{\hat{a},\hat{a}^\dagger}(n)$ and plot the corresponding fidelity in the insets of Fig. 4. The fidelities decrease with increasing n because, for high photon-number states, the overlap with the probe states is low and hence the experimental data do not provide sufficient information about the effect of the process on these states [15]. As a result, for each tensor element that has a relatively large value, we observe small, but not negligible, values for the neighboring tensor elements.

Other primary factors contributing to systematic errors in the process tensor estimations include the local oscillator phase estimation uncertainty and the variation of the mode-matching efficiency T_2 between experimental runs. In addition, the reconstructed tensor is affected by the statistical uncertainties of quadrature probability density measurements. In order to evaluate them, we simulate multiple quadrature statistics data sets in each of which the number of occurrences in each quadrature-phase bin [15] is randomly varied within its standard deviation. Each of these data sets is then used to reconstruct a process tensor, and the collection of tensors obtained in this fashion is analyzed to extract the standard deviation for each tensor element. These standard deviations turn out to not exceed an absolute value of 0.2, with the largest elements of the process tensor exhibiting the highest uncertainties.

Summary.—We use the technique of coherent-state quantum-process tomography to explicitly evaluate, for the first time, the tensors of quantum optical photon creation and annihilation processes. The reconstructed tensors exhibit raising and lowering properties of these operations. This is the first experiment in which complete tomography of trace-nonpreserving quantum processes has been carried out.

We thank B. Sanders, A. Steinberg, and C. Simon for helpful discussions and A. J. Hendricks, A. Chandra, A. Fedorov, and A. S. Prasad for help in the lab. We acknowledge financial support from NSERC and CIFAR.

*LVOV@ucalgary.ca

[1] P. A. M. Dirac, Proc. R. Soc. A **114**, 243 (1927).
[2] M. Barbieri, N. Spagnolo, M. G. Genoni, F. Ferreyrol, R. Blandino, M. G. A. Paris, P. Grangier, and R. Tualle-Brouri, Phys. Rev. A **82**, 063833 (2010).
[3] C. Navarrete-Benlloch, R. García-Patrón, J. H. Shapiro, and N. J. Cerf, Phys. Rev. A **86**, 012328 (2012).
[4] See Supplemental Material at http://link.aps.org/supplemental/10.1103/PhysRevLett.110.130403 for the theoretical background, the method of calibrating probe state amplitudes, and Wigner functions of process output states.
[5] A. Zavatta, S. Viciani, and M. Bellini, Science **306**, 660 (2004).

[6] A. Ourjoumtsev, R. Tualle-Brouri, J. Laurat, and P. Grangier, Science **312**, 83 (2006).
[7] J. S. Neergaard-Nielsen, M. Takeuchi, K. Wakui, H. Takahashi, K. Hayasaka, M. Takeoka, and M. Sasaki, Phys. Rev. Lett. **105**, 053602 (2010).
[8] V. Parigi, A. Zavatta, M. S. Kim, and M. Bellini, Science **317**, 1890 (2007).
[9] H. Takahashi, J. S. Neergaard-Nielsen, M. Takeuchi, M. Takeoka, K. Hayasaka, A. Furusawa, and M. Sasaki, Nat. Photonics **4**, 178 (2010).
[10] S. Gleyzes, S. Kuhr, C. Guerlin, J. Bernu, S. Deléglise, U. B. Hoff, M. Brune, J.-M. Raimond, and S. Haroche, Nature (London) **446**, 297 (2007).
[11] U. Leonhardt, *Measuring the Quantum State of Light* (Cambridge University Press, Cambridge, England, 1997).
[12] A. I. Lvovsky and M. G. Raymer, Rev. Mod. Phys. **81**, 299 (2009).
[13] M. Lobino, D. Korystov, C. Kupchak, E. Figueroa, B. C. Sanders, and A. I. Lvovsky, Science **322**, 563 (2008).
[14] S. Rahimi-Keshari, A. Scherer, A. Mann, A. T. Rezakhani, A. I. Lvovsky, and B. C. Sanders, New J. Phys. **13**, 013006 (2011).
[15] A. Anis and A. I. Lvovsky, New J. Phys. **14**, 105021 (2012).
[16] M. Lobino, C. Kupchak, E. Figueroa, and A. I. Lvovsky, Phys. Rev. Lett. **102**, 203601 (2009).
[17] J. S. Lundeen, A. Feito, H. Coldenstrodt-Ronge, K. L. Pregnell, Ch. Silberhorn, T. C. Ralph, J. Eisert, M. B. Plenio, and I. A. Walmsley, Nat. Phys. **5**, 27 (2009).
[18] L. Zhang, H. B. Coldenstrodt-Ronge, A. Datta, G. Puentes, J. S. Lundeen, X.-M. Jin, B. J. Smith, M. B. Plenio, and I. A. Walmsley, Nat. Photonics **6**, 364 (2012).
[19] G. Brida, L. Ciavarella, I. P. Degiovanni, M. Genovese, L. Lolli, M. G. Mingolla, F. Piacentini, M. Rajteri, E. Taralli, and M. G. A. Paris, New J. Phys. **14**, 085001 (2012).
[20] L. Zhang, A. Datta, H. B. Coldenstrodt-Ronge, X.-M. Jin, J. Eisert, M. B. Plenio, and I. A. Walmsley, New J. Phys. **14**, 115005 (2012).
[21] F. Ferreyrol, N. Spagnolo, R. Blandino, M. Barbieri, and R. Tualle-Brouri, Phys. Rev. A **86**, 062327 (2012).
[22] R. Kumar, E. Barrios, A. MacRae, E. Cairns, E. H. Huntington, and A. I. Lvovsky, Opt. Commun. **285**, 5259 (2012).
[23] Y. Chi, B. Qi, W. Zhu, L. Qian, H.-K. Lo, S.-H. Youn, A. I. Lvovsky, and L. Tian, New J. Phys. **13**, 013003 (2011).
[24] S. R. Huismann, N. Jain, S. A. Babichev, F. Vewinger, A. N. Zhang, S. H. Youn, and A. I. Lvovsky, Opt. Lett. **34**, 2739 (2009).
[25] E. Bimbard, N. Jain, A. MacRae, and A. I. Lvovsky, Nat. Photonics **4**, 243 (2010).
[26] G. S. Agarwal and K. Tara, Phys. Rev. A **43**, 492 (1991).
[27] Z. Hradil, J. Řeháček, J. Fiurášek, and M. Ježek, in *Quantum State Estimation*, edited by M. G. A. Paris and J. Řeháček (Springer, Berlin, 2004).
[28] A. I. Lvovsky, J. Opt. B **6**, S556 (2004).
[29] J. Rehacek, Z. Hradil, E. Knill, and A. I. Lvovsky, Phys. Rev. A **75**, 042108 (2007).
[30] J. Řeháček, D. Mogilevtsev, and Z. Hradil, Phys. Rev. Lett. **105**, 010402 (2010).
[31] J. Appel, D. Hoffman, E. Figueroa, and A. I. Lvovsky, Phys. Rev. A **75**, 035802 (2007).
[32] T. Aichele, A. I. Lvovsky, and S. Schiller, Eur. Phys. J. D **18**, 237 (2002).
[33] A. I. Lvovsky, H. Hansen, T. Aichele, O. Benson, J. Mlynek, and S. Schiller, Phys. Rev. Lett. **87**, 050402 (2001).